Arl13b and the exocyst interact synergistically in ciliogenesis

Cecília Seixas[a,*], Soo Young Choi[b,*], Noemi Polgar[c], Nicole L. Umberger[d], Michael P. East[e], Xiaofeng Zuo[b], Hugo Moreiras[a], Rania Ghossoub[f], Alexandre Benmerah[g,h], Richard A. Kahn[e], Ben Fogelgren[c], Tamara Caspary[d,†], Joshua H. Lipschutz[b,i,†], and Duarte C. Barral[a,†]

[a]CEDOC, NOVA Medical School/Faculdade de Ciências Médicas, Universidade Nova de Lisboa, 1169-056 Lisbon, Portugal; [b]Department of Medicine, Medical University of South Carolina, Charleston, SC 29425; [c]Department of Anatomy, Biochemistry, and Physiology, John A. Burns School of Medicine, University of Hawaii at Manoa, Honolulu, HI 96813; [d]Department of Human Genetics and [e]Department of Biochemistry, Emory University School of Medicine, Atlanta, GA 30022; [f]Centre de Recherche en Cancérologie de Marseille, INSERM, UMR7258, 13009 Marseille, France; [g]INSERM UMR 1163, Laboratory of Inherited Kidney Diseases, 75015 Paris, France; [h]Paris Descartes-Sorbonne Paris Cité University, Imagine Institute, 75015 Paris, France; [i]Department of Medicine, RHJ Veterans Affairs Medical Center, Charleston, SC 29425

ABSTRACT **Arl13b belongs to the ADP-ribosylation factor family within the Ras superfamily of regulatory GTPases. Mutations in Arl13b cause Joubert syndrome, which is characterized by congenital cerebellar ataxia, hypotonia, oculomotor apraxia, and mental retardation. Arl13b is highly enriched in cilia and is required for ciliogenesis in multiple organs. Nevertheless, the precise role of Arl13b remains elusive. Here we report that the exocyst subunits Sec8, Exo70, and Sec5 bind preferentially to the GTP-bound form of Arl13b, consistent with the exocyst being an effector of Arl13b. Moreover, we show that Arl13b binds directly to Sec8 and Sec5. In zebrafish, depletion of *arl13b* or the exocyst subunit *sec10* causes phenotypes characteristic of defective cilia, such as curly tail up, edema, and abnormal pronephric kidney development. We explored this further and found a synergistic genetic interaction between *arl13b* and *sec10* morphants in cilia-dependent phenotypes. Through conditional deletion of *Arl13b* or *Sec10* in mice, we found kidney cysts and decreased ciliogenesis in cells surrounding the cysts. Moreover, we observed a decrease in Arl13b expression in the kidneys from Sec10 conditional knockout mice. Taken together, our results indicate that Arl13b and the exocyst function together in the same pathway leading to functional cilia.**

Monitoring Editor
Wallace Marshall
University of California, San Francisco

Received: Feb 25, 2015
Revised: Oct 29, 2015
Accepted: Nov 12, 2015

INTRODUCTION

Primary cilia are microtubule-based organelles that protrude from the surface of most eukaryotic cells. They operate as antenna-like structures, detecting and transmitting endocrine, chemical, and mechanical signals from the extracellular environment to the intracellular space. Their correct assembly and sensory functions are crucial for embryonic and postnatal development, as well as for tissue

This article was published online ahead of print in MBoC in Press (http://www.molbiolcell.org/cgi/doi/10.1091/mbc.E15-02-0061) on November 18, 2015.

*These authors contributed equally to this work.

†These authors supervised the work equally.

C.S. performed immunoprecipitations, affinity chromatography purification, the direct interaction assay, and the immunofluorescence in mammalian cell lines, under the supervision of D.C.B.; H.M. performed immunoprecipitations, under the supervision of D.C.B.; N.L.U. performed the mouse crosses, genotyping, and kidney dissections, under the supervision of T.C.; S.Y.C. performed the experiments using zebrafish, as well as the immunohistochemistry, immunofluorescence, and immunoblotting analysis of mouse kidneys together with X.Z., under the supervision of J.H.L.; M.P.E. designed experiments and performed the purification of Arl13b-GST under the supervision of R.A.K.; R.G. performed immunofluorescence in RPE1 cells, under the supervision of A.B.; P.N. performed the mouse crosses, genotyping, and kidney dissections of Sec10 conditional knockout mice, under the supervision of B.F.; the manuscript was written by C.S. and D.C.B.

Address correspondence to: Duarte C. Barral (duarte.barral@nms.unl.pt), Cecília Seixas (cecilia.seixas@nms.unl.pt).

Abbreviations used: ERC, endocytic recycling compartment; *hnn*, *hennin*; MO, morpholino.

homeostasis in adulthood. Indeed, defects in this organelle lead to several human diseases collectively known as ciliopathies (Badano *et al.*, 2006).

Several small G proteins within the Ras superfamily are implicated in primary cilia assembly, particularly in the regulation of ciliary cargo traffic. These include members of the Rab and ADP-ribosylation factor (Arf) families, which regulate all steps of vesicular trafficking, including vesicle formation and transport, as well as tethering/docking and fusion with acceptor compartments (Das and Guo, 2011; Donaldson and Jackson, 2011). Small G proteins function as molecular switches, alternating between GDP- and GTP-bound states. When GTP bound, they are considered active and can bind to effectors that mediate a variety of downstream functions.

Ciliary proteins are synthesized in the cytosol and then trafficked from intracellular compartments to primary cilia via membrane traffic pathways. One of the pathways postulated relies on endocytic recycling (Nachury *et al.*, 2010). Indeed, Rab17 and Rab11 are believed to regulate cargo traffic from the endocytic recycling compartment (ERC) to the primary cilium (Yoshimura *et al.*, 2007; Westlake *et al.*, 2011). In addition, several Arf family members, including Arl3, Arl6, and Arl13b, are associated with the primary cilium (Li *et al.*, 2012). When mutated, Arl6 causes Bardet–Biedl syndrome (BBS), a ciliopathy characterized by retinal dystrophy, renal dysfunction, obesity, and polydactyly, among other defects (Blacque and Leroux, 2006). Moreover, Arl6 is proposed to regulate ciliary cargo traffic by recruiting a multisubunit complex, termed the BBSome, to the base of the cilium (Li *et al.*, 2012).

ARL13B is mutated in families affected by the classical form of Joubert syndrome (Cantagrel *et al.*, 2008; Thomas *et al.*, 2014). This ciliopathy is characterized by congenital cerebellar ataxia, hypotonia, oculomotor apraxia, and mental retardation, as well as a distinctive neurological imaging feature known as the "molar tooth sign" (Romani *et al.*, 2013). Zebrafish *arl13b* mutants (also known as *scorpion* [*sco*]) display pronephric cysts and abnormal cilia formation in multiple organs (Sun *et al.*, 2004; Duldulao *et al.*, 2009), and mouse *Arl13b*-null (also known as *hennin* [*hnn*]) mutant embryos exhibit perturbed ciliogenesis and Sonic hedgehog (Shh) signaling (Caspary *et al.*, 2007). Although Arl13b is highly enriched in the ciliary membrane, the mechanism by which Arl13b regulates ciliogenesis remains unclear (Larkins *et al.*, 2011; Li *et al.*, 2012). Moreover, we showed that Arl13b regulates the trafficking of cargo endocytosed independently of clathrin through the ERC (Barral *et al.*, 2012), but the link between this function and the role of Arl13b in cilia biogenesis, if any, has yet to be established.

On the other hand, ciliogenesis and proper localization of ciliary proteins, such as polycystin-2, are known to be regulated by proteins of the exocyst complex (Zuo *et al.*, 2009; Fogelgren *et al.*, 2011). Originally characterized in yeast as a complex of eight subunits (Sec3, Sec5, Sec6, Sec8, Sec10, Sec15, Exo70, and Exo84), the exocyst is involved in the tethering/docking of vesicles from the *trans*-Golgi network (TGN) and the ERC to acceptor compartments (He and Guo, 2009). The exocyst complex is an effector of Rab11, an ERC marker (Zhang *et al.*, 2004), and Sec4, which is homologous to mammalian Rab8 (Guo *et al.*, 1999). In addition, the exocyst subunit Sec10 is a downstream effector of Arf6, which recruits the exocyst from the ERC to the plasma membrane to promote membrane recycling toward specialized membrane regions (Prigent *et al.*, 2003). Depletion of the exocyst leads to abnormal cystogenesis in three-dimensional cell culture (Zuo *et al.*, 2009), and overexpression of the exocyst subunit Sec15 leads to the clustering of ERC-derived vesicles and impairs the formation of primary cilia (Feng *et al.*, 2012). Of importance, a mutation in *EXOC8*, encoding the exocyst subunit Exo84, was found recently in a family with the classical form of Joubert syndrome (Dixon-Salazar *et al.*, 2012), raising the possibility that Arl13b and the exocyst function in the same pathway.

Here, we provide biochemical and genetic evidence, the latter from both mouse and zebrafish, supporting functional interactions between Arl13b and the exocyst complex. Specifically, we show that Arl13b interacts with the exocyst via the Sec8 and Sec5 subunits when in its active GTP-bound form, suggesting that the exocyst is an effector of Arl13b. We also find that, in zebrafish, *arl13b* and *sec10* display a synergistic genetic interaction in several cilia-dependent phenotypes. Moreover, we show that the conditional deletion of *Arl13b* or *Sec10* in mice leads to cystic kidneys and decreased ciliogenesis in kidney epithelia, further suggesting a functional linkage between this small G protein and the exocyst complex.

RESULTS

Arl13b interacts with the exocyst complex

Mutations in *EXOC8* or *ARL13B* lead to Joubert syndrome in human families (Cantagrel *et al.*, 2008; Dixon-Salazar *et al.*, 2012), suggesting a link between the exocyst and Arl13b. Therefore, we investigated whether the exocyst complex physically interacts with Arl13b. To this end, we immunoprecipitated protein extracts of mouse inner medullary collecting duct (IMCD3) cells with a rabbit antibody raised against Arl13b (Barral *et al.*, 2012) and probed for the presence of the Sec8 subunit of the exocyst. Because small G proteins preferentially bind their effectors when in the GTP-bound, active state, we incubated protein extracts with GTPγS, a nonhydrolyzable form of GTP, before performing the immunoprecipitations. For comparison, we used samples preincubated with GDP. We found that preincubation with GTPγS dramatically increases the coimmunoprecipitation of Sec8 with Arl13b compared with the GDP control (Figure 1A). In the case of immunoprecipitation with an irrelevant rabbit immunoglobulin G (IgG) antibody, we observed a fainter band for Sec8, likely caused by Sec8 binding nonspecifically to the beads in our immunoprecipitations (Figure 1A). The finding that Sec8 coimmunoprecipitates with Arl13b in a GTPγS-sensitive manner is consistent with an interaction between Arl13b and Sec8.

To investigate whether Arl13b coimmunoprecipitates with other subunits of the exocyst complex, we immunoblotted for the Exo70 and Sec5 subunits after immunoprecipitating Arl13b in ciliated IMCD3 cell extracts. We found that both Sec5 and Exo70 coimmunoprecipitate with Arl13b, suggesting that Arl13b may interact with the entire exocyst complex (Figure 1B). We also tested for the interaction between Arl13b and exocyst subunits in another ciliated cell type, NIH-3T3 mouse embryonic fibroblasts, and were able to confirm that Sec8, Exo70, and Sec5 exhibit a GTP-dependent interaction with Arl13b (Figure 1C). Furthermore, we immunoprecipitated Arl13b from nonciliated HeLa cells and found that Sec8 and Sec5 are also enriched in the precipitates in a GTPγS-sensitive manner, indicating that the interaction is conserved and not dependent upon the presence of cilia (Supplemental Figure S1). Of note, although we consistently observed these exocyst subunits to be specifically immunoprecipitated with antibodies to Arl13b and preferentially after incubation with GTPγS, there were differences in the extent of the coprecipitations and sensitivities to GTPγS. These may result from partial dissociation of one or more subunits during coprecipitation or the presence in cells of some subunits that are not fully assembled into the exocyst complex.

We also used the reverse strategy, that is, we immunoprecipitated Sec8 from total cell lysates of ciliated IMCD3 cells in the presence of GTPγS or GDP and detected Arl13b by immunoblotting, confirming the GTPγS-dependent interaction between these two

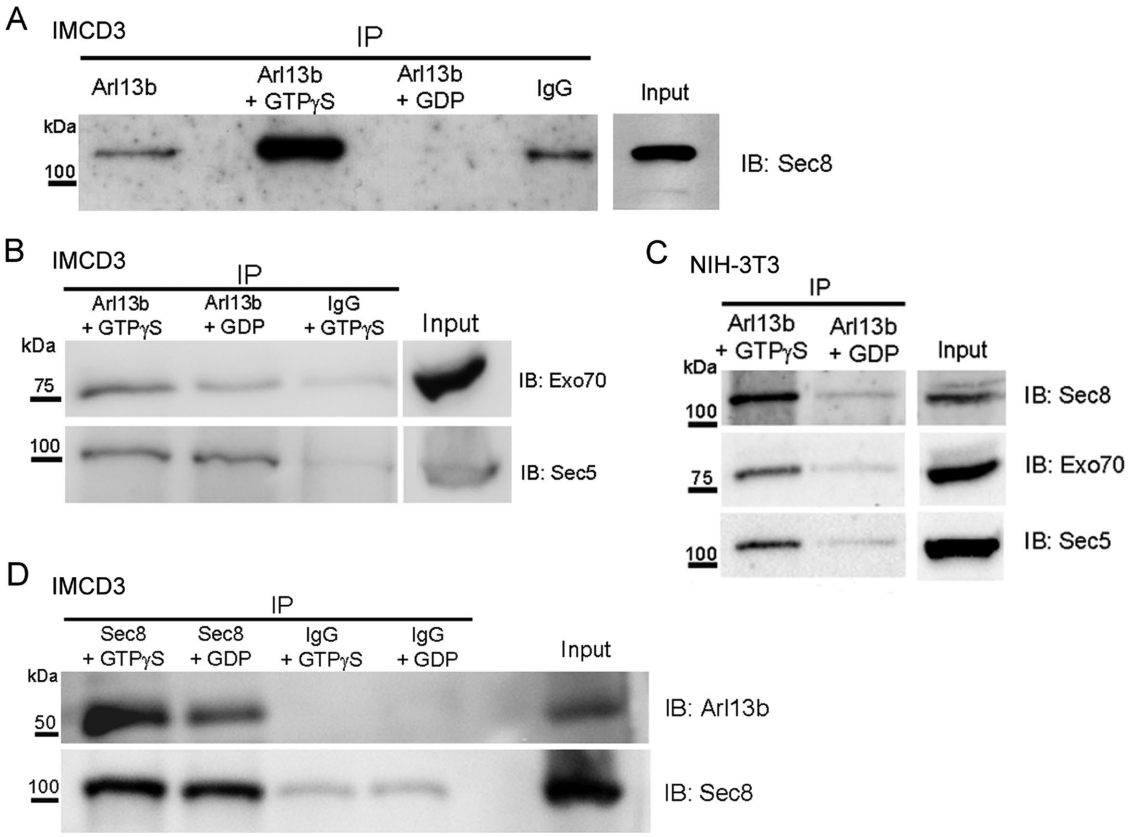

FIGURE 1: Arl13b interacts with the exocyst in ciliated cells. (A) Endogenous Arl13b was immunoprecipitated from cell lysates of ciliated IMCD3 cells after preincubation with either no nucleotide (left lane), GTPγS (second lane), or GDP (third lane). Nonspecific rabbit IgG was used as a negative control (fourth lane). Input is shown in the far right lane. Immunoprecipitates were resolved by SDS–PAGE and immunoblotted with Sec8 antibody. (B) Cell lysates of ciliated IMCD3 cells were immunoprecipitated with Arl13b after preincubation with GTPγS or GDP. Nonspecific rabbit IgG was used as a negative control. Immunoprecipitates were resolved by SDS–PAGE and immunoblotted with Exo70 or Sec5 antibodies. (C) Total cell lysates of ciliated NIH-3T3 cells were immunoprecipitated and analyzed as described in A. (D) Cell lysates of ciliated IMCD3 cells were immunoprecipitated with Sec8 antibody after incubation with GTPγS. An irrelevant mouse IgG1 (IgG) was used as a negative control. Immunoprecipitates were analyzed by SDS–PAGE and immunoblotted with Arl13b antibody. Results are representative of three independent experiments.

proteins (Figure 1D). Taken together, these findings strongly suggest that Arl13b and the exocyst interact and that this interaction is enhanced by the presence of GTPγS, consistent with the exocyst being an effector of Arl13b.

Arl13b interacts directly with Sec8 and Sec5

We next asked with which subunit(s) Arl13b interacts directly. For this, we translated Sec8-Myc and Arl13b-FLAG separately in vitro by a transcription and translation (TNT) T7 polymerase–coupled reticulocyte lysate system, using plasmids encoding the tagged proteins as templates. The fidelity of this system to generate the tagged proteins in vitro was confirmed by immunoblotting (Figure 2A). We found that rabbit reticulocytes have endogenous Sec8 that can be distinguished from the in vitro–translated Sec8 by immunoblotting with anti-Sec8 and anti-Myc antibodies (Figure 2A). The in vitro–translated proteins were then mixed and incubated in the presence of GTPγS. Immunoprecipitation was performed with anti-FLAG monoclonal antibody, and the immunoprecipitated products were analyzed by immunoblot with anti-Myc antibody. The in vitro–translated Sec8-Myc could be detected as coimmunoprecipitating with Arl13b-FLAG, and because the other subunits were not similarly expressed, we conclude that the interaction between Sec8 and Arl13b is likely direct (Figure 2B, asterisk). By immunoblotting with anti-Sec8 antibody, we were able to distinguish the immunoprecipitated in vitro–translated Sec8-Myc from the endogenous Sec8 present in the rabbit reticulocyte (Figure 2B). As a negative control, we performed the immunoprecipitation with an irrelevant IgG. In this case, we detected a faint band by immunoblotting with anti-Myc that most likely corresponds to Sec8-Myc bound nonspecifically to the beads. We also performed an immunoprecipitation with anti-FLAG antibody using as input a mixture of in vitro–translated Arl13b-FLAG with a TNT reaction in which no DNA was added as template. As expected, we detected no band by immunoblotting with anti-Myc antibody. Thus, our data support a direct interaction between Arl13b and Sec8.

Using the same approach, we extended our analysis to other exocyst subunits, namely Sec3, Sec5, Sec15, and Exo70. These proteins were also produced in vitro (Figure 2C) and, as previously described for Sec8, were mixed with Arl13b-FLAG in the presence of GTPγS and subjected to immunoprecipitation with anti-FLAG and immunoblotting with anti-Myc. As a positive control, we performed a reaction with Sec8-Myc. Surprisingly, we found that Sec5-Myc can also interact directly with Arl13b-FLAG (Figure 2D). The lack of evidence for direct binding between Arl13b and Sec3 or Exo70 in

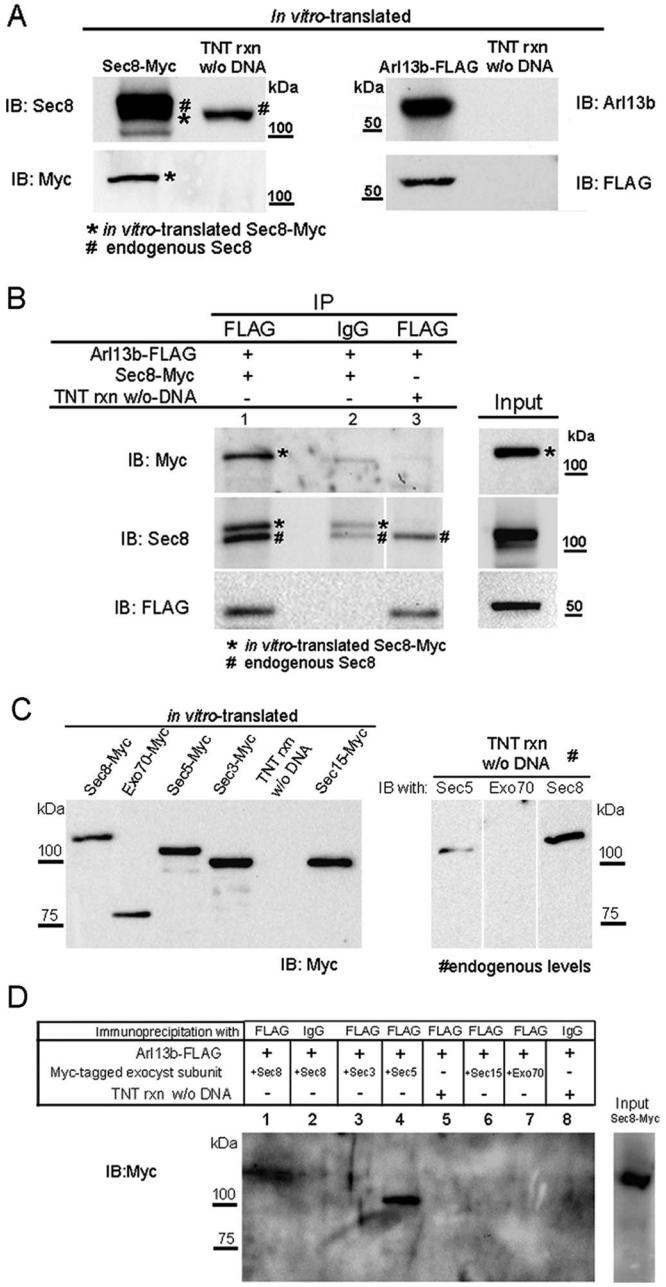

FIGURE 2: Arl13b interacts with the exocyst through the Sec5 and Sec8 subunits. (A) Sec8-Myc and Arl13b-FLAG were in vitro–translated using TNT T7 coupled reticulocyte lysate system. Five percent of the TNT reaction was resolved by SDS–PAGE and analyzed by immunoblotting with Sec8, Myc, Arl13b, or FLAG antibodies. As a control, a TNT reaction without DNA as template was performed and subsequently used in the immunoprecipitations to distinguish the in vitro–translated from the endogenous protein present in the reticulocyte lysate. (B) Immunoprecipitation with FLAG antibody was performed using the in vitro–translated proteins in the presence of GTPγS. Immunoprecipitates (lane 1) were analyzed by immunoblot with Myc, Sec8, or FLAG antibodies. As a negative control, immunoprecipitations were performed with an irrelevant mouse IgG1 (IgG; lane 2). In addition, as a control, immunoprecipitation with FLAG antibody was performed using as input a mixture of a TNT reaction made without DNA and the in vitro–translated Arl13b-FLAG in the presence of GTPγS (lane 3). Asterisks indicate in vitro–translated Sec8-Myc, and the pound signs indicate endogenous Sec8. (C) Left, Myc-tagged Sec3, Sec5, Sec8, Sec15, and Exo70 exocyst subunits were in vitro translated using the TNT system. Five percent of the TNT reaction was resolved by SDS–PAGE and analyzed by immunoblotting with Myc antibody. Right, endogenous levels of Sec5, Sec8, and Exo70 present on 5% of the TNT reaction were analyzed by immunoblotting with specific antibodies for each subunit. (D) Immunoprecipitation with FLAG antibody was performed using the in vitro–translated proteins described in C, in the presence of GTPγS. Immunoprecipitates were analyzed by immunoblot with Myc antibody or silver staining. Negative controls (lanes 2, 5. and 8) were performed as in B. Results are representative of three independent experiments.

this assay is further evidence of specificity for its association with Sec8 and Sec5.

To further test for the direct binding of Sec8 and Sec5 with Arl13b, we purified by affinity chromatography identical amounts of in vitro–translated Myc-tagged Sec8 or Sec5, using glyoxal agarose beads cross-linked to anti-Myc antibody. As a negative control, we used in vitro–translated Exo70-Myc, which, according to our results, does not interact directly with Arl13b (Figure 2D). We successfully eluted the Myc-tagged exocyst subunits, as shown in Supplemental Figure S2A. The purity was confirmed by silver staining (Supplemental Figure 2B). Next we cross-linked anti–glutathione *S*-transferase (GST) antibody to the agarose beads and incubated with Arl13b-GST and then with identical amounts of purified Sec5-, Sec8- or Exo70-Myc, always in the presence of GTPγS. As a negative control, we used anti-GST–coupled beads incubated with purified Sec8 and anti-GST–coupled beads incubated with purified GST and then with purified exocyst subunits, also in the presence of GTPγS (Figure 3). The eluted products were analyzed by immunoblotting with anti-Myc or subjected to silver staining. The results confirm that Sec8 and Sec5 interact directly with Arl13b-GST, in contrast with Exo70, which is not detected in the eluted products. We detected a faint band in the negative control corresponding to Sec5 that likely represents nonspecific binding to the beads. Nevertheless, this band is much weaker than the band corresponding to Sec5 binding to Arl13b-GST. Of importance, the silver staining shows that equal amounts of Arl13b-GST were used in all conditions.

Arl13b and the exocyst colocalize in cilia and the periciliary region

To test whether the interaction between Arl13b and the exocyst could be related to ciliary functions, we used confocal microscopy to analyze the localization of different exocyst subunits, either staining endogenous levels with specific antibodies or overexpressing tagged forms. We observed Sec8 colocalizing with Arl13b along cilia in polarized Madin–Darby canine kidney cells (MDCKs; Figure 4, A–C), as well as in an hTERT-immortalized retinal pigment epithelial cell line (RPE-1; Figure 4, D–F). In NIH-3T3 cells, overexpressed Sec5-HA also colocalizes with endogenous Arl13b along cilia (Figure 4, G–I and inset). Moreover, Sec5-HA was observed at the ciliary base of these cells (Figure 4, J–L and inset). In addition, overexpressed mCherry-tagged Sec10, Exo70, and Exo84 localize to the periciliary region (Figure 4, M–O and inset, and Supplemental Figure S3).

arl13b and *sec10* interact synergistically in cilia-related phenotypes

Because we found biochemical evidence linking Arl13b and the exocyst complex, both of which play crucial roles in development, we decided to analyze this interaction in vivo to investigate its effect on organ development. Because Sec8 depletion in mice causes

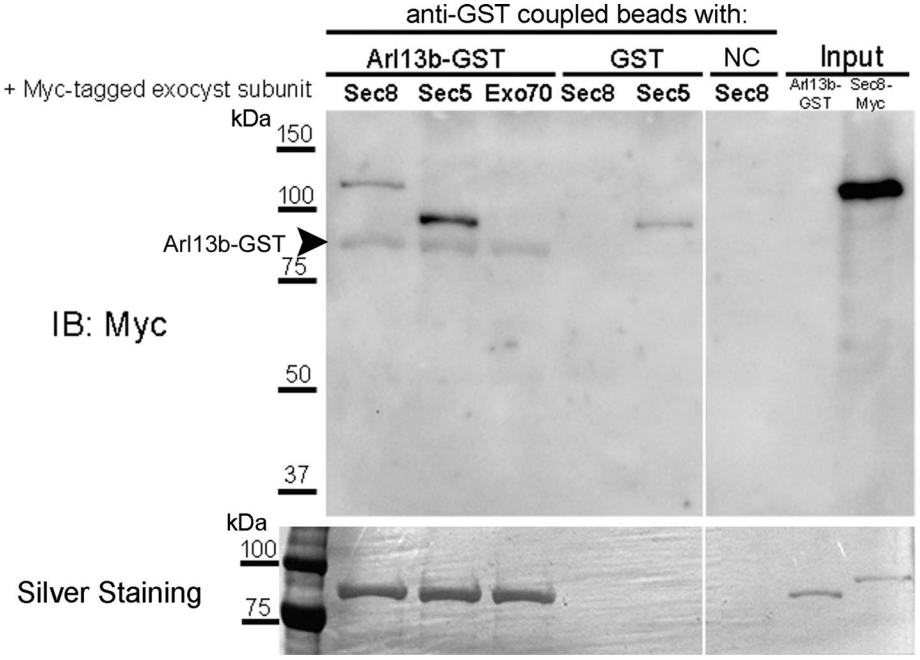

FIGURE 3: Arl13b interacts directly with Sec5 and Sec8 exocyst subunits. Purified Myc-tagged, in vitro–translated Sec5, Sec8, or Exo70 was mixed with anti–GST-coupled agarose beads previously incubated with purified Arl13b-GST or GST. A negative control (NC) to detect nonspecific binding of exocyst subunits to the agarose beads was added, in which anti–GST-coupled beads were directly incubated with purified Sec8-Myc protein. Eluted products were analyzed by SDS–PAGE, followed by immunoblotting for Myc tag or silver staining. The latter shows that identical amounts of purified Arl13b-GST were incubated in the different conditions. The membrane was previously probed with GST antibody to detect Arl13b-GST (arrowhead). Five percent of the purified proteins used in the assay was run in the input. Results are representative of at least two independent experiments.

early embryonic lethality (Friedrich *et al.*, 1997) and the Sec10 subunit is considered to be the core subunit of the exocyst complex (Roth *et al.*, 1998; Zuo *et al.*, 2009), we decided to deplete both *arl13b* and *sec10* using antisense morpholinos (MOs) in zebrafish.

The morphants for either *arl13b/sco* or the exocyst subunit *sec10* lead to ciliary phenotypes already described (Sun *et al.*, 2004; Duldulao *et al.*, 2009; Fogelgren *et al.*, 2011). A synergistic genetic interaction usually reflects mutations in functionally related genes; it can be identified when the contribution of two mutations to the phenotype of a double mutant exceeds the additive effects of the individual mutations. We therefore injected *sec10* or *arl13b* MOs at suboptimal doses that do not result in abnormal phenotypes on their own (Figure 5). Whereas injections of *arl13b* MO at either 1 or 2 ng yield no significant changes in phenotype compared with dye-injected controls, when we combined this with a suboptimal dose of 7.5 ng of s*ec10* MO, we observed a significant increase in the percentage of abnormal phenotypes. Similarly, injection of 7.5 ng of *sec10* MO alone shows a weak effect (~10% abnormal embryos), whereas we scored 22% abnormal embryos when we injected 1 ng of *arl13b* MO plus 7.5 ng of *sec10* MO and 49.3% with the combination of 2 ng of *arl13b* MO with 7.5 ng of *sec10* MO. Abnormal phenotypes resulting from coinjections of these MOs include curved tail, small eyes, and pericardial edema (Figure 5, A–H), which occur when there is impaired ciliary function (Kramer-Zucker *et al.*, 2005; Fogelgren *et al.*, 2011; Lee *et al.*, 2012).

Thus, as shown in the graph in Figure 5I, when we coinjected both MOs at suboptimal doses, we observed a striking synergistic effect on cilia-related phenotypes. These data further argue that Arl13b and the exocyst function together in cilia-related processes during zebrafish development.

Conditional deletion of Arl13b in kidney results in increased organ size with large cysts

A hallmark of many ciliopathies is the presence of cystic kidneys. We know that Arl13b is important for kidney development in zebrafish, since the *arl13b*^{sco} mutants display cystic kidneys (Sun *et al.*, 2004; Duldulao *et al.*, 2009). Because mammals have a complex metanephric kidney compared with the zebrafish pronephros, we decided to explore whether Arl13b has a role in mammalian kidney development.

Because *Arl13b*^{hnn} mice are embryonic lethal at day 13.5–14.5 (Caspary *et al.*, 2007), we analyzed *Arl13b*$^{floxed//floxed}$ (*Arl13b*$^{FL/FL}$) mice crossed with a *Nestin-Cre* (*Nes-Cre*) strain, which is expressed in the nervous system and certain segments of the kidney tubules (Tronche *et al.*, 1999; Dubois *et al.*, 2006; Su *et al.*, 2012). At postnatal day 7 (P7), we found that the kidneys of *Arl13b*$^{FL/FL}$*;Nes-Cre* mice are grossly enlarged compared with those of control littermates (Figure 6A). Hematoxylin and eosin–stained sections from the kidneys of *Arl13b*$^{FL/FL}$*;Nes-Cre* mice revealed many large cysts (Figure 6, B and B′). To identify the tubular origins of the cysts, we stained the *Arl13b*$^{FL/FL}$*;Nes-Cre* and control kidneys with three different lectins: *Lotus tetragonolobus* agglutinin (LTA), peanut agglutinin (PNA), and *Dolichos biflorus* agglutinin (DBA), which label the proximal tubules, distal tubules, and collecting ducts, respectively. Cysts in the kidneys of *Arl13b*$^{FL/FL}$*;Nes-Cre* mice originate from all segments of the nephron, which is consistent with the expression pattern of the *Nestin-Cre* driver (Figure 6C; Dubois *et al.*, 2006). Thus, our analysis of the kidneys from *Arl13b*$^{FL/F}$*;Nes-Cre* mice further supports the idea that Arl13b is important for the development of metanephric kidneys.

Conditional deletion of Arl13b inhibits ciliogenesis in the kidney and activates the mitogen-activated protein kinase and Hippo pathways

To determine whether Arl13b plays a role in the formation of renal primary cilia, we analyzed kidney sections for the presence of ciliary Arl13b. We identified cilia using antibodies against acetylated α-tubulin (Figure 7A, arrows). In the kidneys of *Arl13b*$^{FL/FL}$*;Nes-Cre* mice, there is a near absence of cilia in cells lining the cysts (Figure 7A′, arrowhead). In contrast, normal-appearing tubules, where *Nestin-Cre* is likely not expressed, display primary cilia positive for both Arl13b and acetylated tubulin (Figure 7A, arrow). Indeed, by quantifying the acetylated α-tubulin staining, we found a decrease in the number of cells displaying cilia in the cyst cells (10.6%) compared with unaffected cells (85.5%; Figure 7B).

To determine which signaling pathways are activated after Arl13b depletion, we examined the mitogen-activated protein kinase (MAPK) pathway because it is known to be deregulated in cyst epithelium (Omori *et al.*, 2006) and polycystic kidney disease (PKD),

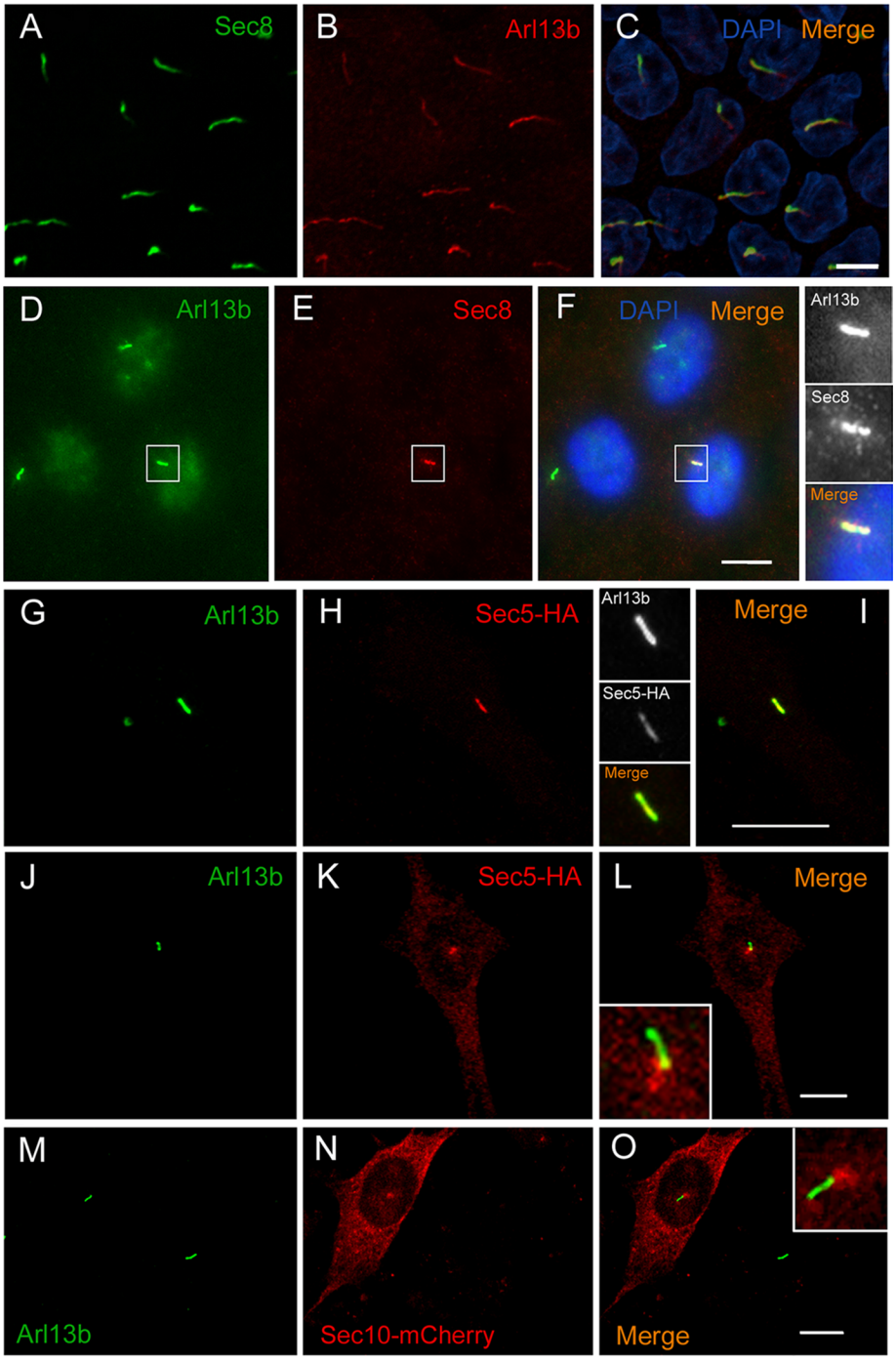

FIGURE 4: Arl13b colocalizes with the exocyst in cilia and the periciliary region. (A–C) Sec8 (green) colocalizes with Arl13b (red) along cilia of polarized MDCK cells. DAPI stains nuclei (blue). (D–F) In RPE1 cells, Sec8 (red) colocalizes with Arl13b (green) along cilia. Insets, higher magnification of the cilium staining. (G–I) In NIH-3T3 cells, Sec5-HA (red) colocalizes with Arl13b (green) along cilia. Insets, higher magnification of cilia showing colocalization of Sec5-HA and Arl13b. (J–L) Sec5-HA (red) is also found accumulated in the base of cilia marked by Arl13b (green) in NIH-3T3 cells. Inset, higher magnification of the periciliary region. (M–O) In NIH-3T3 cells, Sec10-mCherry accumulates in the base of cilia marked by Arl13b (green). Inset, higher magnification of the periciliary region. Scale bar, 5 μm (A–C), 10 μm (D–O).

leading in the latter case to aberrant cell proliferation (Lawrence *et al.*, 2008). We evaluated the levels of activated extracellular signal–regulated kinase (phosphorylated pERK), a key protein in the MAPK signaling cascade, in kidney lysates from P7 and P11 *Arl13b*$^{FL/FL}$;*Nes-Cre* mice and compared them with levels in wild-type mice (Figure 7C). We observed an increase in pERK levels in the *Arl13b*$^{FL/FL}$;*Nes-Cre* mice, indicating that the MAPK signaling pathway is upregulated. We also evaluated the activation of another pathway that is frequently associated with cancer (Harvey *et al.*, 2013), the Hippo pathway, by immunoblotting with an anti–transcriptional coactivator with PDZ-binding motif (TAZ) antibody, which is a key indicator for activation of this pathway. *Arl13b*$^{FL/FL}$;*Nes-Cre* kidneys show increased TAZ levels at P7 and P11. In contrast, we saw no differences in Sec8 or Sec10 protein levels in control versus *Arl13b*$^{FL/FL}$;*Nes-Cre* kidneys.

Conditional deletion of Sec10 in kidney epithelia results in a cystic kidney phenotype with decreased Arl13b expression

To further study in vivo the functional relationship between Arl13b and the exocyst in kidney development and homeostasis, we analyzed the kidneys of Sec10 conditional deletion mice. For this, we used our recently generated transgenic mouse line with a conditional floxed Sec10 allele (Sec10$^{FL/FL;}$ Fogelgren *et al.*, 2015; Polgar *et al.*, 2015). We crossed the floxed-Sec10 mice with the Ksp1.3-Cre strain, which expresses Cre recombinase in epithelial cells from distal and collecting tubules, derived from the ureteric bud (Shao *et al.*, 2002), resulting in offspring with a kidney-specific conditional deletion of Sec10 (Sec10$^{FL/FL}$;Ksp-Cre). Although most of the Sec10$^{FL/FL}$;Ksp-Cre knockouts develop in utero bilateral ureter obstruction and die as newborns (Fogelgren *et al.*, 2015), the remaining animals can survive to adulthood. Kidneys from 10-wk-old Sec10$^{FL/FL}$ control and Sec10$^{FL/FL}$;Ksp-Cre conditional deletion animals were collected, and macroscopic changes in kidney appearance were readily observed in the knockout animals (Supplemental Figure S4A). The adult Sec10$^{FL/FL}$;Ksp-Cre kidneys have a variable phenotype, which ranges from a smaller fibrotic kidney with numerous smaller cysts to an enlarged kidney with much bigger cysts (Supplemental Figure S4B). Kidneys from control littermates (Sec10$^{FL/FL}$) always appear normal. A dramatic increase of smooth muscle actin in Sec10 conditional deletion kidneys was detected upon immunofluorescence staining (Supplemental Figure S4C), confirming increased fibrogenesis. We previously measured significantly fewer renal cilia in Sec10-knockout tubules (Polgar *et al.*, 2015), and the cilia that remained were much shorter, with a stubby appearance. To determine whether Arl13b subcellular localization changes as a result of Sec10 deletion,

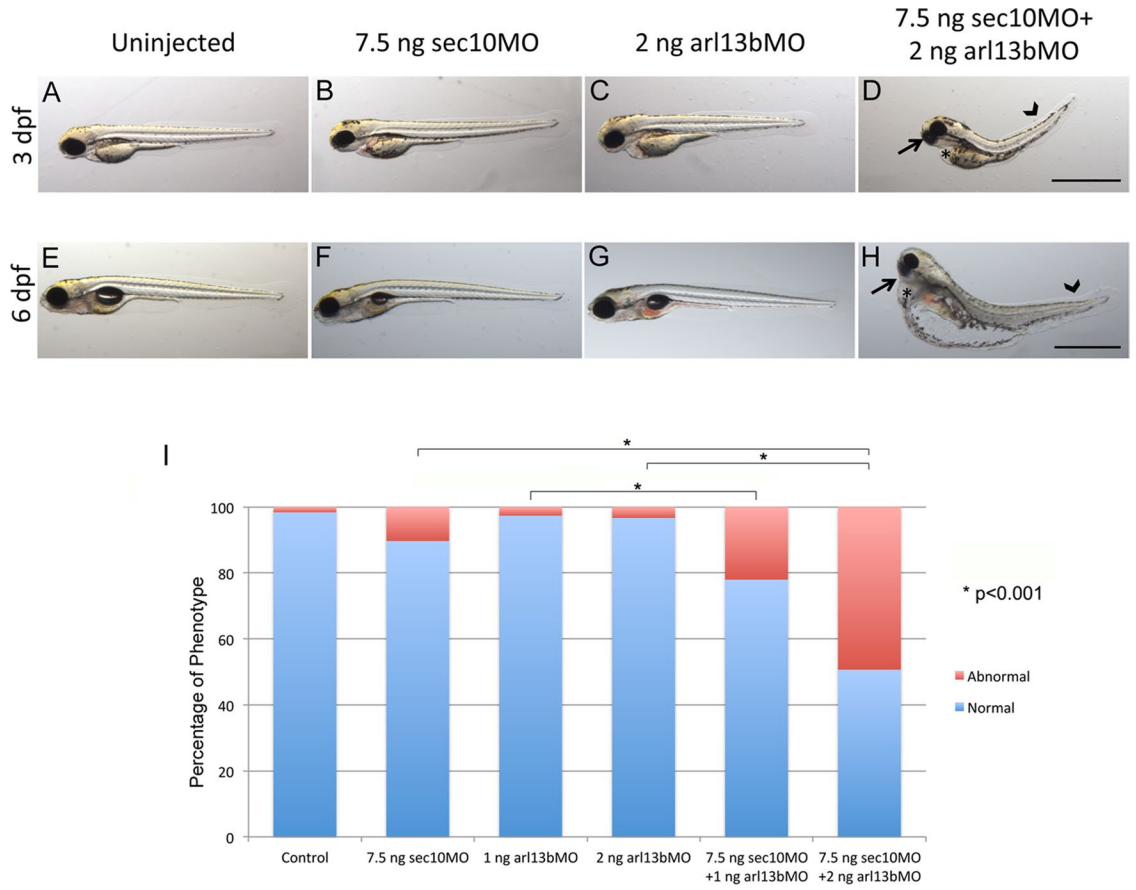

FIGURE 5: *arl13b* and *sec10* interact synergistically in cilia-related phenotypes. (A–H) Gross phenotypes of zebrafish embryo morphants at 3 d postfertilization (dpf) (A–D) and 6 dpf (E–H), on lateral view, after injection of MOs for *arl13b* and/or *sec10*. A synergistic interaction resulting in small eyes (arrow), pericardial edema (asterisk), and tail curvature (arrowhead) was observed upon coinjection of suboptimal doses of 2 ng of *arl13b* MO plus 7.5 ng of *sec10* MO at both 3 and 6 dpf (D and H, respectively), which do not result in an abnormal phenotype when injected alone (B, C, F, and G); $n = 535$. (I) Histogram showing quantification of the effect of MOs at 3 dpf. Coinjection of suboptimal doses of 2 ng of *arl13b* MO plus 7.5 ng of *sec10* MO results in a significant increase in the percentage of abnormal phenotypes (*$p < 0.001$) compared with injection of the MO alone (2 ng of *arl13b* MO or 7.5 ng of *sec10* MO). Scale bars, 1 mm.

we analyzed these adult kidneys by immunostaining and confocal microscopy. In Sec10$^{FL/FL}$;Ksp-Cre kidneys, Arl13b colocalizes with the primary cilia marker acetylated tubulin on the shortened cilia, similar to controls (Figure 8A). When overall Arl13b protein levels from total protein extracts of Sec10$^{FL/FL}$ control and Sec10$^{FL/FL}$;Ksp-Cre knockout kidneys were compared by immunoblotting, the latter show significantly lower protein expression (Figure 8B).

DISCUSSION

Arl13b was first identified as a regulator of cilia and kidney development in zebrafish (Sun *et al.*, 2004) and subsequently studied for its role in cilia structure and Shh signaling in mice (Caspary *et al.*, 2007; Duldulao *et al.*, 2009; Larkins *et al.*, 2011). We now present evidence that Arl13b interacts with the exocyst via the Sec5 and Sec8 subunits. The exocyst is a hetero-octameric complex best known for its function in tethering and spatial targeting of exocytic vesicles to the plasma membrane. Because only the Sec10 and Sec15 exocyst subunits are known to exist in free pools in the cell, possibly forming a subcomplex in addition to their incorporation in the complex (Guo *et al.*, 1999), we propose that Arl13b interacts with the entire exocyst complex. This conclusion is supported by the coimmunoprecipitation of Sec8, Sec5, and Exo70 with Arl13b.

We show that Arl13b interacts with the exocyst complex in a GTPγS-sensitive manner, suggesting that the exocyst is a downstream effector of Arl13b in mammalian cells. We previously found that Arl13b regulates endocytic recycling traffic (Barral *et al.*, 2012), but a direct link between the role of Arl13b in endocytic recycling and its function in ciliogenesis has not yet been established. Several studies indicate the ERC can serve as a donor compartment for ciliary-bound cargo (Nachury *et al.*, 2010). Moreover, the TGN and the ERC have been implicated in the trafficking of rhodopsin transport carriers to cilia-derived photoreceptor-rod outer segments in retinal cells, under the control of Rab11 and Arf4 (Mazelova *et al.*, 2009a,b). In addition, Rab11 and Rab8, together with the Rab guanine nucleotide exchange factor Rabin8, are recruited to the ciliary-bound post-TGN vesicular carriers, and, via interaction with the exocyst, ensure the tethering of these carriers to the periciliary plasma membrane (Knödler *et al.*, 2010; Westlake *et al.*, 2011; Feng *et al.*, 2012; Wang *et al.*, 2012). Of interest, several subunits of the exocyst, such as Sec6, Sec8, and Sec10, have been localized to the cilium or the base of this organelle in mammalian cell lines (Rogers *et al.*, 2004; Zuo *et al.*, 2009; Babbey *et al.*, 2010). In addition, silencing of the Sec10 exocyst subunit leads to a decrease in primary ciliogenesis (Zuo *et al.*, 2009; Fogelgren *et al.*, 2011). Here, we show that Sec5 localizes to both

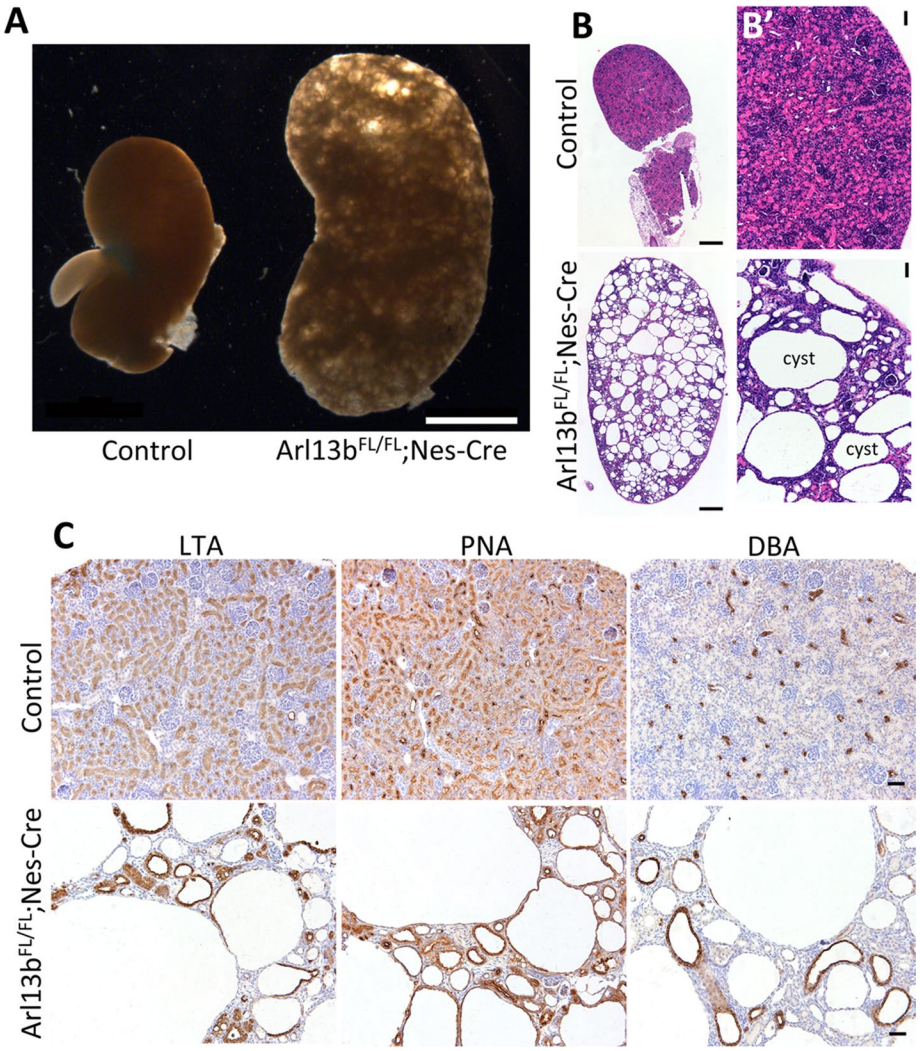

FIGURE 6: Conditional deletion of Arl13b in murine kidneys leads to the formation of cysts originating from different kidney tubule segments. (A) Images of kidneys from mice with a conditional deletion of Arl13b (*Arl13b$^{FL/FL}$;Nes-Cre*), compared with a control littermate. (B, B′) Hematoxylin and eosin stainings of fixed sections from kidneys of control mice and mice with conditional deletion of Arl13b. (C) Kidney sections from control mice (top) or mice with conditional deletion of Arl13b (bottom) incubated with LTA lectin, which stains the apical membrane of proximal tubule epithelial cells; PNA lectin, which stains both distal and collecting tubules; and DBA lectin, which exclusively stains the collecting ducts. Scale bars, 2 mm (A), 200 µm (B), 20 µm (B′, C).

cilia and the periciliary region and Exo70 and Exo84 to the periciliary region. Note that, contrary to polarized MDCK cells, Sec8 and Sec5 are not found in all Arl13b-positive cilia of RPE1 and NIH-3T3 cells, respectively. This could be explained by the timing of ciliogenesis, since the cells were not synchronized. Although the cells were starved at the same time to induce ciliation, the absence of synchronization implies that cilia formation occurs at different times. This could lead to a difference in the localization of the exocyst subunits, especially if the complex participates in cilia formation. Thus, on the basis of these findings, we hypothesized that the interaction of Arl13b with the exocyst would have implications for ciliogenesis. To test our hypothesis, we performed functional studies in zebrafish *arl13b/sec10* double-morphant embryos, which revealed a synergistic genetic interaction between Arl13b and Sec10 on cilia-related phenotypes. Moreover, we found that the conditional deletion of *Arl13b* or *Sec10* in mouse kidneys leads to a similar phenotype, with kidney cysts and decreased ciliogenesis in kidney tubule epithelia. Taken together, these findings point to a model in which Arl13b regulates the trafficking of vesicles containing ciliary cargo from the ERC via binding to the exocyst and consequent incorporation of ciliary cargo into the ciliary membrane. Of interest, a similar role was proposed for Rab10, which colocalizes at the base of nascent cilia with exocyst subunits and forms a complex with Sec8 (Babbey *et al.*, 2010). In *Caenorhabditis elegans*, ARL-13 is required for proper targeting/retention of ciliary membrane proteins (Cevik *et al.*, 2010). In mice, Arl13b is needed for the normal distribution of the ciliary G protein–coupled receptor Smoothened and serotonin receptor 6 within cilia (Larkins *et al.*, 2011; Higginbotham *et al.*, 2012). We also present evidence of a direct interaction between Arl13b and two different exocyst subunits, namely Sec5 and Sec8. The functional relevance of this bivalent GTP-dependent interaction remains to be determined, but it could have implications for the selection of cargo molecules, as is the case with Arf1, which interacts directly with multiple subunits of COPI or AP-1 (Yu *et al.*, 2012).

Kidney cyst formation is a hallmark of many ciliopathies. The characterization of several ciliary proteins, such as the nephronophthisis proteins, has been fundamental to understanding cystogenesis as a result of ciliary dysfunction (Hildebrandt *et al.*, 2009; Gascue *et al.*, 2011). Arl13b was cloned as a novel cystic kidney gene named *sco* in zebrafish, and was found to be required for cilia formation in the kidney tubules in this organism (Sun *et al.*, 2004; Duldulao *et al.*, 2009). We now report that postnatal deletion of mouse *Arl13b* in metanephric kidneys affects the formation of cilia and leads to activation of both the MAPK and Hippo pathways, as shown by the up-regulation of pERK and TAZ, respectively. Moreover, the cysts observed in *Arl13b$^{FL/FL}$;Nes-Cre* mice are consistent with a PKD-like phenotype. We also show that the conditional deletion of Sec10 in adult mouse metanephric kidneys causes a similar PKD-like phenotype, characterized by cystic kidneys with decreased ciliogenesis in epithelia. Thus, we propose that depletion of Arl13b or the exocyst, by impairing cilia formation, leads to cyst formation in metanephric kidneys. Of interest, we observed that Arl13b expression is decreased in Sec10 conditional knockout mouse kidneys, suggesting that the exocyst is required for the stability of Arl13b. Alternatively, the absence of cilia could lead to a decreased expression or stability of Arl13b.

Whereas Joubert syndrome–related disorders can be associated with renal defects, and mice lacking Arl13b in kidneys display renal cysts (our data shown here), patients identified with *ARL13B* mutations have no kidney anomalies, although it is possible that they may develop renal abnormalities later in life

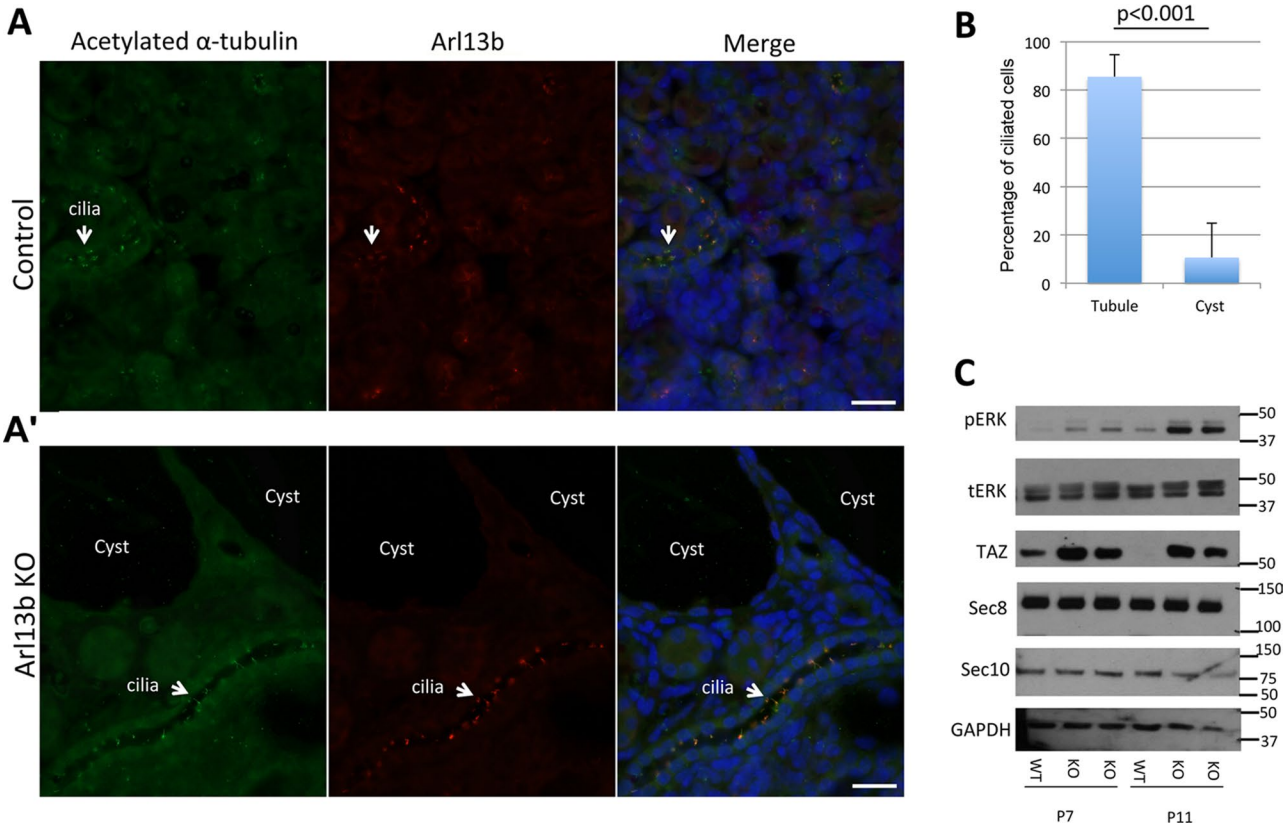

FIGURE 7: Arl13b conditional deletion inhibits ciliogenesis in the kidney and results in increased activation of the MAPK and Hippo pathways. (A, A′) Immunostaining of acetylated α-tubulin (red) and Arl13b (green) in kidneys from control mice (A) and mice with conditional deletion, *Arl13b*$^{FL/FL}$*;Nes-Cre* (A′) at P7. The *Arl13b*$^{FL/FL}$*;Nes-Cre* mutants lack cilia in cells surrounding the cysts, whereas cilia are present in normal-appearing tubules. (B) Quantification of ciliated cells from kidneys of *Arl13b*$^{FL/FL}$*;Nes-Cre* mice shows a significant decrease in the number of cilia per cell in cysts compared with normal-appearing tubules ($n = 325$ cilia). Error bars represent SD. (C) Increased pERK and TAZ levels in *Arl13b*$^{FL/FL}$*;Nes-Cre* mice. Immunoblot analysis of total cell extracts from whole kidneys of control mice and *Arl13b*$^{FL/FL}$*;Nes-Cre* mice at P7 and P11 with phosphorylated ERK (pERK), total ERK (tERK), TAZ, Sec8, Sec10, or GAPDH antibodies. Note that distinct *Arl13b*$^{FL/FL}$*;Nes-Cre* mice were analyzed at P7 and P11. Results are representative of four independent experiments. Scale bars, 10 μm.

(Cantagrel *et al.*, 2008). Alternatively, the nature of the alleles may explain the difference; the patient mutations are point mutations and so are likely hypomorphic alleles, whereas the mouse *Arl13b* conditional deletion leads to a protein-null allele. Similarly, the mutation in Exo84 that was reported in a Joubert syndrome patient does not involve renal defects. We speculate that if mutations in both Arl13b and a subunit of the exocyst occurred simultaneously, the patients would exhibit a more severe phenotype likely involving renal defects, similar to the zebrafish double morphants. In addition, as with other small G proteins, Arl13b is likely to possess multiple effectors whose interaction may be disrupted by mutations in distinct residues of the GTP-binding domain (Joneson *et al.*, 1996; Kuai and Kahn, 2000). Indeed, we have shown that Arl13b also interacts with the nonmuscle myosin heavy chain IIA (Casalou *et al.*, 2014). Thus the patient mutations identified may disrupt effectors unrelated to the kidney phenotypes caused by the absence of Arl13b protein. This means that distinct mutations in *ARL13B* may lead to distinct constellations of Joubert syndrome–related phenotypes or other ciliopathies.

In conclusion, our study reveals a novel effector of Arl13b—the exocyst—and suggests that these proteins function in the same pathway that is required for proper ciliogenesis.

MATERIALS AND METHODS

Cell culture and transfection

HeLa cells were cultured at 37°C and 5% CO_2, in DMEM (Invitrogen, Paisley, UK) supplemented with 10% fetal bovine serum (FBS; Invitrogen), 100 U/ml penicillin G, 100 μg/ml streptomycin, 2 mM L-glutamine, and 20 mM 4-(2-hydroxyethyl)-1-piperazineethanesulfonic acid (HEPES; Invitrogen). NIH-3T3 cells were maintained in the same conditions and medium but supplemented with 10% bovine calf serum (Sigma-Aldrich, St. Louis, MO). Murine IMCD3 and human RPE1 cells were cultured in DMEM:F-12 supplemented with 10% FBS, 100 U/ml penicillin G, 100 μg/ml streptomycin, 2 mM L-glutamine, and 20 mM HEPES (Invitrogen). To stimulate ciliogenesis, NIH-3T3 cells were serum-starved for 24 h in 0.5% bovine serum albumin (BSA)–containing medium, and RPE1 and IMCD3 cells were serum-starved for 48 h in 0.2% FBS-containing medium. Transfections were performed using Lipofectamine 2000 (Invitrogen) for RPE1 or Turbofect (Thermo Scientific, Waltham, MA) for NIH-3T3 according to the manufacturer's instructions and processed for immunofluorescence after 24 h.

Zebrafish injections and morpholino knockdown

Embryos were injected at the one- to four-cell stage, and morpholinos were diluted with phenol red tracer (Sigma-Aldrich) at 0.05%

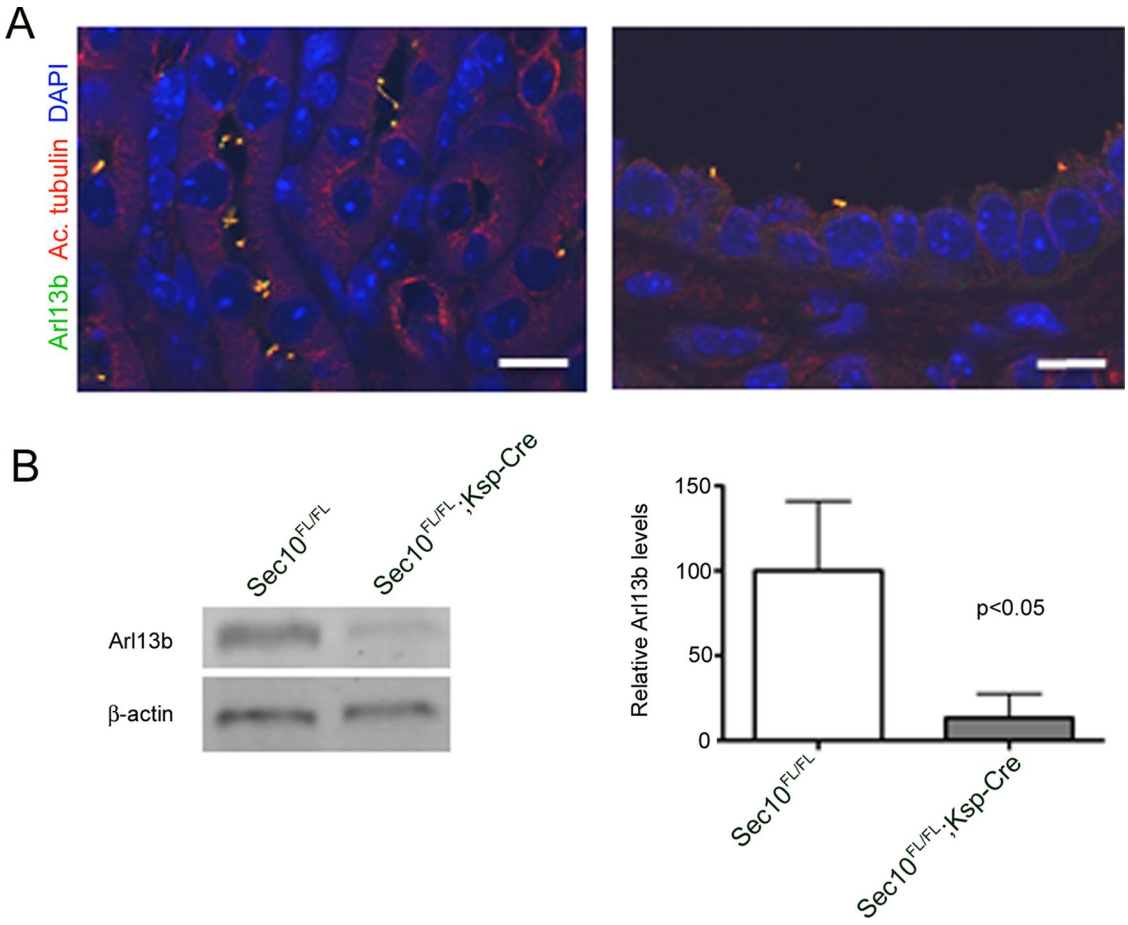

FIGURE 8: Kidney-specific Sec10 conditional knockout results in ciliary defects and decreased Arl13b levels. (A) Immunofluorescence staining of adult kidney tubules of kidney-specific Sec10$^{FL/FL}$;Ksp-Cre conditional knockout mouse for Arl13b (green) and the primary cilia marker acetylated α-tubulin (red). Cilia are fewer and shorter in Sec10-depleted tubules, although some Arl13b is still detected in the abnormal primary cilia. Scale bar, 10 μm. (B) Overall, Arl13b protein levels are dramatically decreased in Sec10$^{FL/FL}$;Ksp-Cre kidneys compared with Sec10$^{FL/FL}$ controls, as measured by immunoblotting.

final concentration and injected at 500 pl or 1 nl/embryo. The *arl13b*AUG morpholino (*arl13b MO*) was a kind gift of Zhaoxia Sun (Yale University School of Medicine, New Haven, CT) and was used to block the translation of *arl13b* (Sun *et al.*, 2004). *Sec10*e2i2 morpholino (*Sec10 MO*) was designed to target the exon 2/intron 2 boundary and was described previously (Fogelgren *et al.*, 2011). Morpholinos were injected either as single doses of 1 or 2 ng of *arl13b* MO and 7.5 ng of *sec10* MO or a combined dose of 1 or 2 ng of *arl13b* MO plus 7.5 ng of *sec10* MO (designated in the text as "1 or 2 ng of *arl13b* MO plus 7.5 ng of *sec10* MO") per embryo. As a control, uninjected or phenol red tracer–injected embryos were analyzed at the same stage. Embryos were imaged using a Leica M205C Light Microscope. Images were captured in TIFF format and processed in Adobe Photoshop CS5.1.

Immunoblotting of mouse kidney lysates

Kidneys from control mice or mice with conditional deletion of *Arl13b* at day 7 or 11 after birth were homogenized in RIPA buffer (Sigma-Aldrich) containing protease and phosphatase inhibitors, and the lysates were centrifuged at 12,000 × *g* for 20 min at 4°C. Supernatants were collected and protein concentration was determined using the bicinchoninic acid protein assay (Thermo Scientific). The protein samples were loaded onto NuPage 4–12% Bis-Tris gels (Thermo Scientific) and then transferred to a nitrocellulose membrane. The membranes were subjected to immunoblotting, followed by immunodetection using an Amersham Bioscience ECL Detection Kit. Protein extracts from kidneys of 10-wk-old Sec10$^{FL/FL}$;Ksp-Cre knockout and Sec10$^{FL/FL}$ control mice (Fogelgren *et al.*, 2015) were prepared similarly to the Arl13b-depleted kidneys. The samples were separated on SDS–PAGE and then transferred to polyvinylidene fluoride (PVDF) membranes. The membranes were subjected to standard immunoblotting, and immunodetection and quantification of band intensities were performed using an Odyssey CLx Infrared Imaging System from LI-COR Biosciences.

Immunofluorescence

Immunostaining of MDCK cells grown on Transwell filters was performed as previously described (Zuo *et al.*, 2009), except that the cells were fixed with 4% paraformaldehyde for 15 min at 37°C. The NIH-3T3 and RPE1 cells were fixed with 4% paraformaldehyde on ice at 4°C for 30 min and then incubated with primary antibodies diluted in phosphate-buffered saline (PBS) with 0.1% Triton and 1 mg/ml BSA for 1 h at room temperature. Secondary antibodies were incubated in PBS with 1 mg/ml BSA for 30 min at room temperature. Coverslips were mounted in mounting medium (15% [wt/vol] Vinol 205, 33% [vol/vol] glycerol, 0.1% azide in PBS) and analyzed in a Zeiss LSM 710 confocal microscope equipped with a Plan-Apochromat 63/1.40 Oil Ph3 lens.

Antibodies

The antibodies used in immunoblotting were mouse anti-Myc clone 9E10 (Millipore, Darmstadt, Germany), mouse anti-Sec10 (Zuo *et al.*, 2009), mouse anti-rSec8 (Enzo Life Sciences, East Farmingdale, NY), mouse anti-Exo70 (Millipore), rabbit anti-Sec5 (NovusBio, Cambridge, UK), rabbit anti-Arl13b (Proteintech, Chicago, IL), goat anti-Arl13b (Santa Cruz Biotechnology, Paso Robles, CA), anti–β-actin (Cell Signaling, Beverly, MA), mouse anti–FLAG M2 (Sigma-Aldrich), rabbit anti-TAZ (Cell Signaling), rabbit anti–phospho-ERK1/2 (Cell Signaling), rabbit anti–total ERK1/2 (Cell Signaling), mouse anti–glyceraldehyde-3-phosphate dehydrogenase (GAPDH; Sigma-Aldrich), mouse anti–acetylated α-tubulin (Sigma-Aldrich), and affinity-purified rabbit anti-Arl13b (Barral *et al.*, 2012). Mouse and rabbit IgG (Sigma-Aldrich) were used as IgG controls in the immunoprecipitations. For immunofluorescence of Arl13b-depleted kidney sections, rabbit anti-Arl13b (Caspary *et al.*, 2007) and mouse anti–acetylated α-tubulin (Sigma-Aldrich) were used with Cy2- or Cy3-conjugated anti-rabbit or anti-mouse secondary antibodies (Jackson ImmunoResearch Laboratories, West Grove, PA). Sec10-depleted kidneys were stained with mouse anti–α-smooth muscle actin (Sigma-Aldrich) and rabbit anti–E-cadherin (Cell Signaling) with, respectively, DyLight 594 anti-mouse and DyLight 488 anti-rabbit secondary antibodies (Vector Laboratories, Burlingame, CA).

In vitro translation

Myc-tagged Sec3, Sec5, Sec8, and Exo70 were generated from full-length rat cDNA cloned into pGBKT7 as described previously (Zuo *et al.*, 2011). Arl13b-FLAG was generated from full-length mouse Arl13b cDNA cloned into pcDNA3.1 and FLAG-tagged at the C-terminus (Barral *et al.*, 2012). Two micrograms of each plasmid was used per reaction of the TNT T7-coupled in vitro transcription and translation rabbit reticulocyte lysate system (Promega, Madison, WI), following the manufacturer's instructions. The reaction was performed at 25°C for 90 min. The efficiency of the production was evaluated running ~5% of the final volume in SDS–PAGE, followed by transfer to a nitrocellulose membrane and immunoblotting with anti-FLAG, Myc, Arl13b, Sec8, Sec5, or Exo70 antibodies. As a negative control, a reaction without DNA template was performed in the same conditions. The analysis of this control in SDS–PAGE, followed by immunoblotting, was taken as an indication of the endogenous expression levels of the different proteins in the rabbit reticulocyte lysates.

Immunoprecipitation

Cells were lysed in cold lysis buffer (50 mM Tris-HCl, pH 7.4, 1% IGEPAL, 150 mM NaCl, 1 mM EDTA, 1 mM ethylene glycol tetraacetic acid [EGTA], 2 mM $MgCl_2$, 1 mM dithiothreitol [DTT]) in the presence of EDTA-free protease and phosphatase inhibitors for 20 min on ice, followed by centrifugation at 12,000 × *g* for 20 min at 4°C. Protein concentration in total cell lysates was determined using the DC protein assay kit (Bio-Rad, Hercules, CA). For immunoprecipitation, cell lysates (1 mg of protein) were precleared for 1 h with protein G–Sepharose beads (Sigma-Aldrich). GTPγS (0.5 mM; Sigma-Aldrich) or GDP (5 mM; Sigma-Aldrich) was added to the precleared lysates for 15 min at room temperature before immunoprecipitations using 2 μg of anti-Sec8 (Enzo Life Sciences), 3 μg of affinity-purified rabbit polyclonal anti-Arl13b (Barral *et al.*, 2012), 3 μg of anti-FLAG (Sigma-Aldrich), or equal amounts of isotype control IgG for 16 h at 4°C with rotation. Protein G–Sepharose beads were then added and mixed for 5 h at 4°C before being recovered by centrifugation and washed once with lysis buffer with high salt concentration (500 mM NaCl) and then three times with lysis buffer (150 mM NaCl). Immunoprecipitates were finally resuspended in Laemmli sample buffer, boiled at 95°C for 5 min, and resolved by 8% SDS–PAGE, followed by transfer to nitrocellulose membrane and immunoblotting with anti-Arl13b, -Sec8, or -Exo70 antibodies. In the same blot, 5% of the input was resolved by SDS–PAGE and analyzed by immunoblotting.

Affinity coupling of agarose beads and purification of exocyst subunits

The in vitro–translated (IVT) Myc-tagged Sec5, Sec8, and Exo70 proteins were purified by affinity chromatography. For this, 50 μg of goat anti-Myc antibody (Sicgen, Carcavelos, Portugal) was coupled to 100 μl of high-density glyoxal agarose beads (ABT, Madrid, Spain) in sodium bicarbonate buffer, pH 10, overnight at 4°C in a rolling shaker. The binding between the beads and the antibody was stabilized by sodium borohydrate for 30 min at room temperature. Then, anti-Myc-coupled beads were subjected to quenching for 1 h at room temperature with 1 M Tris HCl, pH 7.4. Next, antibody-coupled beads were washed twice with 1 M NaCl and again with 25 mM phosphate buffer, pH 7.4. For each exocyst subunit, 200 μl of the IVT reaction was incubated with 100 μl of anti-Myc–coupled beads in immunoprecipitation buffer (50 mM Tris-HCl, pH 7.4, 1% IGEPAL, 150 mM NaCl, 1 mM EDTA, 1 mM EGTA, 2 mM $MgCl_2$, 1 mM DTT) in the presence of EDTA-free protease and phosphatase inhibitors. Samples were incubated overnight at 4°C in a rolling shaker. Afterward, beads were recovered by centrifugation, washed twice with immunoprecipitation buffer with high salt concentration (500 mM NaCl), and then washed twice with immunoprecipitation buffer. Elution was performed with 0.2 M glycine, pH 2.5, followed by neutralization with 1 M Tris HCl, pH 10. The eluted products were analyzed by SDS–PAGE, followed by immunoblotting with anti-Myc or silver staining.

Purification of murine Arl13b-GST

The complete murine *Arl13b* open reading frame, encoding a protein of 427 residues, was amplified by PCR using primers that introduced *Kpn*I and *Sph*I restriction sites at the 5′ and 3′ ends, respectively, to facilitate subcloning into the pLEXm-GST vector (a generous gift of James Hurley, National Institutes of Health, Bethesda, MD). The pLEXm-GST-ARL13B open reading frame sequence was confirmed, matching NM_026577.3. Human embryonic kidney 293T cells were grown in 10-cm plates in DMEM (GIBCO, Carlsbad, CA) supplemented with 10% FBS (Atlanta Biologicals, Flowery Branch, GA) at 37°C in a humidified environment gassed with 5% CO_2. When the cells reached ~90% confluence, the medium was switched to DMEM with 2% FBS, and cells were transfected with 1 μg of DNA and 3 μg of polyethyleneimine (PEI Max; Polysciences, Warrington, PA)/ml medium. Cells were harvested 48 h after transfection, pelleted by centrifugation at 2000 × *g*, frozen in liquid nitrogen, and stored at –80°C until used for protein purification. Cells were thawed on ice and lysed in five volumes of lysis buffer (50 mM HEPES, pH 7.4, 100 mM NaCl, and 1% 3-[(3-cholamidopropyl)dimethylammonio]-1-propanesulfonate with protease inhibitor cocktail [Sigma-Aldrich] and 10 μg/ml deoxyribonuclease I [Sigma-Aldrich]). The cells were maintained on ice for 30 min before cell debris was removed by centrifugation at 12,000 × *g* for 10 min at 4°C. The GST-ARL13B was purified by addition of 500 μl of glutathione–Sepharose 4B beads (GE Healthcare, Chalfont St. Giles, UK) to 120 mg of protein lysate and incubated at 4°C for 2 h. The beads were washed three times with five column volumes of lysis buffer. Protein was eluted from the beads with three column volumes of elution buffer (25 mM HEPES, pH 7.4, 100 mM NaCl, and 10 mM

glutathione). Eluates were pooled and concentrated using an Amicon spin concentrating unit with a 50-kDa cutoff, with repeated dilution and concentration to remove glutathione and a human embryonic kidney 293T cell contaminant of ~20 kDa.

Direct interaction assay

Anti–GST-coupled glyoxal agarose beads (ABT) were prepared as described (see *Affinity coupling of agarose beads and purification of exocyst subunits*), incubating per sample 50 µg of goat anti-GST antibody (Sicgen) with 100 µl of agarose beads (ABT). Five micrograms of purified Arl13b-GST was mixed with 100 µl of anti-GST coupled beads in immunoprecipitation buffer (50 mM Tris-HCl, pH 7.4, 1% IGEPAL, 150 mM NaCl, 1 mM EDTA, 1 mM EGTA, 2 mM $MgCl_2$, 1 mM DTT, and EDTA-free protease and phosphatase inhibitor) in the presence of GTPγS (0.5 mM; Sigma-Aldrich) at 4°C overnight under constant rolling. Unbound protein was removed by washing the beads twice with immunoprecipitation buffer with high salt concentration (500 mM NaCl) and then twice with immunoprecipitation buffer. Then, pelleted beads were ressuspended to 1 ml of final volume with immunoprecipitation buffer, and identical amounts of purified exocyst subunits were added to each sample and incubated overnight at 4°C under roller shaking, also in the presence of GTPγS. Next, beads were washed as previously and recovered by centrifugation at 12,000 × *g* for 5 min. Beads were resuspended in Laemmli sample buffer and boiled at 95°C for 5 min and the immunoprecipitated products resolved by 8% SDS–PAGE, followed by transfer to PVDF membrane and immunoblotting with anti-Myc antibody or silver staining. In the same blot, 5% of the input was resolved by SDS–PAGE and analyzed either by immunoblotting or silver staining.

Immunohistochemistry and immunofluorescence on kidney sections

For immunohistochemistry, the sections were deparaffinized, and epitope retrieval was performed by heating the sections at 95°C in 10 mM sodium citrate buffer, pH 6.0, for 10 min. After treatment in 0.5% hydrogen peroxide for 5 min at room temperature, the sections were blocked with a streptavidin/biotin blocking kit (SP-2002; Vector Laboratories) and incubated for 30 min with the VECTASTAIN Elite ABC kit (PK-6101 and PK-6102; Vector Laboratories) according to the manufacturer's instructions and counterstained with hematoxylin. Sections were stained with biotinylated LTA, PNA, and DBA (all from Vector Laboratories). For immunofluorescence staining, sections were fixed with 4% paraformaldehyde and paraffin embedded, then dewaxed, rehydrated in graded ethanol, and retrieved with 10 mM sodium citrate, pH 6.0. Sections were blocked in PBS containing 5% donkey serum and then incubated with the primary antibodies in blocking solution overnight at 4°C. After being washed, samples were incubated with the secondary antibodies in the same solution for 1 h at room temperature. 4′,6-Diamidino-2-phenylindole (DAPI) was used to stain nuclei. Coverslips were mounted in KPL mounting medium. Samples were imaged in an Olympus BX42 or a Zeiss Axio Observer D1m microscope. Images were captured in TIFF format and processed in the Adobe Photoshop CS5.1. *Sec10* conditional knockout and control kidneys were analyzed with an Olympus BX41 microscope, using epifluorescence. For detailed analysis of primary cilia, kidney sections were imaged using an Olympus Fluoview1000 confocal microscope.

Statistical analysis

Phenotypes for the epistasis experiments were classified as abnormal after morpholino injection by the presence of any combination of pericardial edema, curly tails, and small eyes. Logistic regression and chi-square testing were used to compare the proportion of abnormal phenotypes across groups. Confidence intervals and *p* values were adjusted for within-trial correlation by clustering at the trial level, and robust SE estimation was generated. These tests were performed using Stata software, version 12.1 (Stata, College Station, TX). For comparison of means, the Student's *t* test was performed using SPSS software (version 15.0). For all tests, $p < 0.05$ was considered statistically significant.

Animal studies

All zebrafish experiments were approved by the Institutional Animal Care and Use Committees at the University of Pennsylvania, the Medical University of South Carolina, and the Philadelphia and Charleston Veterans Affairs Medical Center. All mouse work was performed under the approved guidelines of the Emory University Institutional Animal Care and Use Committee and the University of Hawaii.

ACKNOWLEDGMENTS

We thank Zhaoxia Sun (Yale University School of Medicine, New Haven, CT) for kindly providing the *arl13b* morpholino, Xiao-Wei Chen and Alan R. Saltiel (University of Michigan Medical Center, Ann Arbor, MI) for the Sec5-HA-encoding plasmid, James Hurley (National Institutes of Health, Bethesda, MD) for the plasmid pLEXm-GST, and Jacques Camonis, Maud Hertzog, and Philippe Chavrier (Institut Curie, Paris, France) for their generous help with antibodies for exocyst subunits and for the plasmids encoding Sec10-mCherry and Exo84-mCherry. We also thank José Ramalho (CEDOC, Lisbon, Portugal) for sharing his expertise in affinity coupling assays and reagents, Carsten Janke (Institut Curie) for kindly providing the IMCD3 cell line, and C. T. Strauss for editing the manuscript. This work was supported by a Marie Curie International Reintegration Grant (PIRG05-GA-2009-247726) and a grant from Câmara Municipal de Oeiras to D.C.B., postdoctoral fellowships from the Fundação para a Ciência e a Tecnologia (SFRH/BPD/32323/2006 and iNOVA4Health-UID/Multi/04462/2013) to C.S., and research funding from the National Institute of Neurological Disorders and Stroke (R01 NS056380) to T.C. and from the National Institute of General Medical Sciences (GM090158) to R.A.K. It was also supported by predoctoral fellowships from the American Heart Association (09PRE2140029) to M.P.E.; an Emory PRISM Graduate Teaching Fellows in K-12 Education Fellowship (DGE0536941), an Emory Genetics and Molecular Biology Graduate Program Training Grant (T32GM008490), and an Emory Human Disease Genetics Training Fellowship (T32MH087977) to N.L.U. Funding to J.H.L. was obtained from the Veterans Administration (Merit Award I01 BX000820), the National Institutes of Health (DK069909 and DK070980), and Satellite Healthcare (Norman S. Coplon Extramural Research Grant). Funding for B.F. was obtained from the National Institutes of Health (1K01DK087852, R03DK100738, and P20GM103456-06A1-8293), the March of Dimes (#5-FY14-56), and Pilot and Feasibility Awards, as well as from National Institutes of Health–Designated Research Centers 5G12MD007601 and 5P30DK074038. Funding for A.B. was obtained from the Fondation pour la Recherche Médicale (DEQ20130326532).

REFERENCES

Babbey CM, Bacallao RL, Dunn KW (2010). Rab10 associates with primary cilia and the exocyst complex in renal epithelial cells. Am J Physiol Renal Physiol 299, F495–F506.

Badano JL, Mitsuma N, Beales PL, Katsanis N (2006). The ciliopathies: an emerging class of human genetic disorders. Annu Rev Genomics Hum Genet 7, 125–148.

Barral DC, Garg S, Casalou C, Watts GFM, Sandoval JL, Ramalho JS, Hsu VW, Brenner MB (2012). Arl13b regulates endocytic recycling traffic. Proc Natl Acad Sci USA 109, 21354–21359.

Blacque OE, Leroux MR (2006). Bardet-Biedl syndrome: an emerging pathomechanism of intracellular transport. Cell Mol Life Sci C 63, 2145–2161.
Cantagrel V, Silhavy J, Bielas S (2008). Mutations in the cilia gene ARL13B lead to the classical form of Joubert syndrome. Am J Hum Genet 170–179.
Casalou C, Seixas C, Portelinha A, Pintado P, Barros M, Ramalho JS, Lopes SS, Barral DC (2014). Arl13b and the non-muscle myosin heavy chain IIA are required for circular dorsal ruffle formation and cell migration. J Cell Sci 127, 2709–2722.
Caspary T, Larkins CE, Anderson KV (2007). The graded response to Sonic Hedgehog depends on cilia architecture. Dev Cell 12, 767–778.
Cevik S, Hori Y, Kaplan OI, Kida K, Toivenon T, Foley-Fisher C, Cottell D, Katada T, Kontani K, Blacque OE (2010). Joubert syndrome Arl13b functions at ciliary membranes and stabilizes protein transport in Caenorhabditis elegans. J Cell Biol 188, 953–969.
Das A, Guo W (2011). Rabs and the exocyst in ciliogenesis, tubulogenesis and beyond. Trends Cell Biol 21, 383–386.
Dixon-Salazar TJ, Silhavy JL, Udpa N, Schroth J, Bielas S, Schaffer AE, Olvera J, Bafna V, Zaki MS, Abdel-Salam GH, *et al*. (2012). Exome sequencing can improve diagnosis and alter patient management. Sci Transl Med 4, 138ra78.
Donaldson JG, Jackson CL (2011). ARF family G proteins and their regulators: roles in membrane transport, development and disease. Nat Rev Mol Cell Biol 12, 362–375.
Dubois NC, Hofmann D, Kaloulis K, Bishop JM, Trumpp A (2006). Nestin-Cre transgenic mouse line Nes-Cre1 mediates highly efficient Cre/loxP mediated recombination in the nervous system, kidney, and somite-derived tissues. Genesis 44, 355–360.
Duldulao Na, Lee S, Sun Z (2009). Cilia localization is essential for in vivo functions of the Joubert syndrome protein Arl13b/Scorpion. Development 136, 4033–4042.
Feng S, Knödler A, Ren J, Zhang J, Zhang X, Hong Y, Huang S, Peränen J, Guo W (2012). A Rab8 guanine nucleotide exchange factor-effector interaction network regulates primary ciliogenesis. J Biol Chem 287, 15602–15609.
Fogelgren B, Lin S-Y, Zuo X, Jaffe KM, Park KM, Reichert RJ, Bell PD, Burdine RD, Lipschutz JH (2011). The exocyst protein Sec10 interacts with Polycystin-2 and knockdown causes PKD-phenotypes. PLoS Genet 7, e1001361.
Fogelgren B, Polgar N, Lui VH, Lee AJ, Tamashiro K-K, Napoli JA, Walton CB, Zuo X, Lipschutz JH (2015). Urothelial defects from targeted inactivation of exocyst Sec10 in mice cause ureteropelvic junction obstructions. PLoS One 10, e0129346.
Friedrich Ga, Hildebrand JD, Soriano P (1997). The secretory protein Sec8 is required for paraxial mesoderm formation in the mouse. Dev Biol 192, 364–374.
Gascue C, Katsanis N, Badano J (2011). Cystic diseases of the kidney: ciliary dysfunction and cystogenic mechanisms. Pediatr Nephrol 26, 1181–1195.
Guo W, Roth D, Walch-Solimena C, Novick P (1999). The exocyst is an effector for Sec4p, targeting secretory vesicles to sites of exocytosis. EMBO J 18, 1071–1080.
Harvey KF, Zhang X, Thomas DM (2013). The Hippo pathway and human cancer. Nat Rev Cancer 13, 246–257.
He B, Guo W (2009). The exocyst complex in polarized exocytosis. Curr Opin Cell Biol 21, 537–542.
Higginbotham H, Eom T-Y, Mariani LE, Bachleda A, Hirt J, Gukassyan V, Cusack CL, Lai C, Caspary T, Anton ES (2012). Arl13b in primary cilia regulates the migration and placement of interneurons in the developing cerebral cortex. Dev Cell 23, 925–938.
Hildebrandt F, Attanasio M, Otto E (2009). Nephronophthisis: disease mechanisms of a ciliopathy. J Am Soc Nephrol 20, 23–35.
Joneson T, White MA, Wigler MH, Bar-Sagi D (1996). Stimulation of membrane ruffling and MAP kinase activation by distinct effectors of RAS. Science 271, 810–812.
Knödler A, Feng S, Zhang J, Zhang X, Das A, Peränen J, Guo W (2010). Coordination of Rab8 and Rab11 in primary ciliogenesis. Proc Natl Acad Sci USA 107, 6346–6351.
Kramer-Zucker AG, Olale F, Haycraft CJ, Yoder BK, Schier AF, Drummond Ia (2005). Cilia-driven fluid flow in the zebrafish pronephros, brain and Kupffer's vesicle is required for normal organogenesis. Development 132, 1907–1921.
Kuai J, Kahn Ra (2000). Residues forming a hydrophobic pocket in ARF3 are determinants of GDP dissociation and effector interactions. FEBS Lett 487, 252–256.
Larkins CE, Aviles GDG, East MP, Kahn RA, Caspary T (2011). Arl13b regulates ciliogenesis and the dynamic localization of Shh signaling proteins. Mol Biol Cell 22, 4694–4703.
Lawrence MC, Jivan A, Shao C, Duan L, Goad D, Zaganjor E, Osborne J, McGlynn K, Stippec S, Earnest S, *et al*. (2008). The roles of MAPKs in disease. Cell Res 18, 436–442.
Lee JE, Silhavy JL, Zaki MS, Schroth J, Bielas SL, Marsh SE, Olvera J, Brancati F, Iannicelli M, Ikegami K, *et al*. (2012). CEP41 is mutated in Joubert syndrome and is required for tubulin glutamylation at the cilium. Nat Genet 44, 193–199.
Li Y, Ling K, Hu J (2012). The emerging role of Arf/Arl small GTPases in cilia and ciliopathies. J Cell Biochem 113, 2201–2207.
Mazelova J, Astuto-Gribble L, Inoue H, Tam BM, Schonteich E, Prekeris R, Moritz OL, Randazzo Pa, Deretic D (2009a). Ciliary targeting motif VxPx directs assembly of a trafficking module through Arf4. EMBO J 28, 183–192.
Mazelova J, Ransom N, Astuto-Gribble L, Wilson MC, Deretic D (2009b). Syntaxin 3 and SNAP-25 pairing, regulated by omega-3 docosahexaenoic acid, controls the delivery of rhodopsin for the biogenesis of cilia-derived sensory organelles, the rod outer segments. J Cell Sci 122, 2003–2013.
Nachury MV, Seeley ES, Jin H (2010). Trafficking to the ciliary membrane: how to get across the periciliary diffusion barrier? Annu Rev Cell Dev Biol 26, 59–87.
Omori S, Hida M, Fujita H, Takahashi H, Tanimura S, Kohno M, Awazu M (2006). Extracellular signal-regulated kinase inhibition slows disease progression in mice with polycystic kidney disease. J Am Soc Nephrol 17, 1604–1614.
Polgar N, Lee AJ, Lui VH, Napoli JA, Fogelgren B (2015). The exocyst gene Sec10 regulates renal epithelial monolayer homeostasis and apoptotic sensitivity. Am J Physiol Cell Physiol 309, C190–C201.
Prigent M, Dubois T, Raposo G, Derrien V, Tenza D, Rossé C, Camonis J, Chavrier P (2003). ARF6 controls post-endocytic recycling through its downstream exocyst complex effector. J Cell Biol 163, 1111–1121.
Rogers KK, Wilson PD, Snyder RW, Zhang X, Guo W, Burrow CR, Lipschutz JH (2004). The exocyst localizes to the primary cilium in MDCK cells. Biochem Biophys Res Commun 319, 138–143.
Romani M, Micalizzi A, Valente EM (2013). Joubert syndrome: congenital cerebellar ataxia with the molar tooth. Lancet Neurol 12, 894–905.
Roth D, Guo W, Novick P (1998). Dominant negative alleles of SEC10 reveal distinct domains involved in secretion and morphogenesis in yeast. Mol Biol Cell 9, 1725–1739.
Shao X, Somlo S, Igarashi P (2002). Epithelial-specific Cre/lox recombination in the developing kidney and genitourinary tract. J Am Soc Nephrol 13, 1837–1846.
Su C-Y, Bay SN, Mariani LE, Hillman MJ, Caspary T (2012). Temporal deletion of Arl13b reveals that a mispatterned neural tube corrects cell fate over time. Development 139, 4062–4071.
Sun Z, Amsterdam A, Pazour GJ, Cole DG, Miller MS, Hopkins N (2004). A genetic screen in zebrafish identifies cilia genes as a principal cause of cystic kidney. Development 131, 4085–4093.
Thomas S, Cantagrel V, Mariani L, Serre V, Lee JE, Elkhartoufi N, de Lonlay P, Desguerre I, Munnich A, Boddaert N, *et al*. (2014). Identification of a novel ARL13B variant in a Joubert syndrome-affected patient with retinal impairment and obesity. Eur J Hum Genet 23, 621–627.
Tronche F, Kellendonk C, Kretz O, Gass P, Anlag K, Orban PC, Bock R, Klein R, Schütz G (1999). Disruption of the glucocorticoid receptor gene in the nervous system results in reduced anxiety. Nat Genet 23, 99–103.
Wang J, Morita Y, Mazelova J, Deretic D (2012). The Arf GAP ASAP1 provides a platform to regulate Arf4- and Rab11-Rab8-mediated ciliary receptor targeting. EMBO J 31, 4057–4071.
Westlake CJ, Baye LM, Nachury MV, Wright KJ, Ervin KE, Phu L, Chalouni C, Beck JS, Kirkpatrick DS, Slusarski DC, *et al*. (2011). Primary cilia membrane assembly is initiated by Rab11 and transport protein particle II (TRAPPII) complex-dependent trafficking of Rabin8 to the centrosome. Proc Natl Acad Sci USA 108, 2759–2764.
Yoshimura S-I, Egerer J, Fuchs E, Haas AK, Barr FA (2007). Functional dissection of Rab GTPases involved in primary cilium formation. J Cell Biol 178, 363–369.
Yu X, Breitman M, Goldberg J (2012). A structure-based mechanism for Arf1-dependent recruitment of coatomer to membranes. Cell 148, 530–542.
Zhang X-M, Ellis S, Sriratana A, Mitchell CA, Rowe T (2004). Sec15 is an effector for the Rab11 GTPase in mammalian cells. J Biol Chem 279, 43027–43034.
Zuo X, Fogelgren B, Lipschutz JH (2011). The small GTPase Cdc42 is necessary for primary ciliogenesis in renal tubular epithelial cells. J Biol Chem 286, 22469–22477.
Zuo X, Guo W, Lipschutz J (2009). The exocyst protein Sec10 is necessary for primary ciliogenesis and cystogenesis in vitro. Mol Biol Cell 20, 2522–2529.